ACS OMEGA

http://pubs.acs.org/journal/acsodf

Article

Control of Cluster Structures in Catalyst Inks by a Dispersion Medium

Daozeng Yang, Shaomin Zhu, Yuqing Guo, Haifeng Tang, Daijun Yang, Cunman Zhang, Pingwen Ming,* and Bing Li*

Cite This: *ACS Omega* 2021, 6, 32960−32969

Read Online

ACCESS | Metrics & More | Article Recommendations

ABSTRACT: The cluster structure in the catalyst ink of a proton exchange membrane fuel cell determines its performance. The interaction among solvent, ionomer, and catalyst in ink determines the cluster structure and affects the microstructure and surface morphology of the catalyst layer, which is of great significance to improve the conductivity of the catalyst layer to protons, electrons, and water. First, the dissolved state of the main chain and the side chain of the ionomer in solvent was characterized. The results of relative viscosity, ζ-potential, effective proton fraction, and nuclear magnetic resonance (NMR) showed that the alcohol aqueous solution promoted the stretching electrolysis of the main chain and the side chain of the ionomer more than the pure aqueous solvent, making the ionomer clusters smaller. The rheological test of the ink shows that the pure water solvent ink has the largest cluster and the strongest network structure. Under the test conditions, the clusters in the ink can be reconstructed quickly after breakage through viscous shearing. The addition of alcohols will make the clusters in the ink smaller and the network structure brittle. After the clusters and the network structure are damaged, they will slowly recombine and the viscosity in the ink will gradually recover. Ethanol will minimize the clusters in the ink, and the network structure in the ink is the weakest. The effect of the network strength on the cluster structure is weakened by reducing the solid content in the ink. The amplitude scanning test shows that the network structure in the slurry is almost eliminated after reducing the solid content, the storage modulus of ink with water, 50 wt % isopropyl alcohol (IPA), 50 wt % *n*-propanol (NPA), and 50 wt % ethanol (ET) decreases in turn, as well as the liquid viscosity behavior increases and the cluster particle size in the ink decreases. In conclusion, more dispersed ionomers and alcohol molecules with smaller molecular structures are more conducive to the dispersion of clusters in the ink.

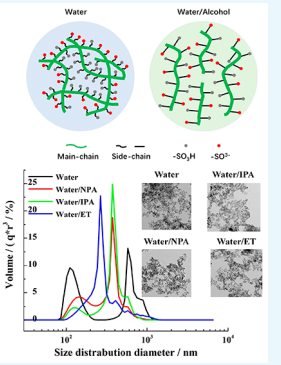

1. INTRODUCTION

A proton exchange membrane fuel cell (PEMFC), as an automobile power source, is known to be the ultimate goal of the development of new energy vehicles and one of the important strategic development plans in China in the future because of its advantages such as low energy consumption, fast fuel filling, and long mileage.[1−3] As an important part of the fuel cell membrane electrode (MEA), a catalyst layer is the place where the electrode redox reaction occurs, which determines the performance and durability of the PEMFC.[4,5] However, the unreasonable structure design of the cathode catalyst layer leads to the challenges of the slow kinetics of oxygen reduction and high mass transfer overpotential.[6−8] As the basic unit of the catalyst layer, the clusters in the catalyst ink have an extremely important impact on the reaction activity, mass transfer, and heat transfer of the catalyst layer.[9−12]

The formation of clusters in the catalyst ink is determined by the interaction between solvent, catalyst, and ionomer.[13] The interaction between the solvent and the ionomer in the ink, and the carbon carrier in the catalyst and Pt crystal has an effect on the structure of the cluster.[14−17] Catalyst particles will undergo secondary agglomeration to form large agglomerated particles under natural conditions.[18−20] The solvent in the catalyst ink is generally a mixture of water and organic solvents. Common organic solvents include alcohols, esters, aldehydes, and acids.[21] The ability of the solvent to invade the carbon carrier depends on the surface energy of carbon support and the surface tension of the solvent. When the surface energy of the solvent is less than that of the carbon support, the solvent can wet the carbon support, which is conducive to the further dispersion of the catalyst aggregate. The surface energy of the Pt crystal is much greater than the surface tension of solvent, which is conducive to the wetting of solvent and the dispersion of catalyst particles. Solvent molecules will interact with the main chain and side chain of the ionomer and dissolve, and $-SO_3H$ of the side chain will be electrolyzed and negatively

Received: September 11, 2021
Accepted: November 10, 2021
Published: November 22, 2021

charged.[22,23] In the catalyst ink, the ionomer will interact with the Pt crystal and the carbon carrier, to adsorb on the catalyst particles, so that the clusters in the catalyst ink can have a negative charge, and the electrostatic repulsion will counteract the van der Waals force between the particles and disperse the particles. According to x-DLVO theory, the Coulomb force and steric hindrance produced by the ionomer on the surface of catalyst clusters affect the particle size and distribution of clusters in the catalyst ink.[24]

The structure of clusters in the ink is related to the solvent and the dispersion of ionomers in the solvent. Welch et al.[22] used small-angle neutron scattering (SANS) and ^{19}F nuclear magnetic resonance (NMR) to prove that Nafion showed three types of structural morphologies: rodlike, solvated large particles (>200 nm), and random coil in glycerol and ethylene glycol, water/isopropanol, and *N*-methyl pyrrolidone solvents. Shimanuki et al.[25] studied the morphology of ionomers by low-temperature transmission electron microscopy (cryo-TEM) and speculated that the dispersion state of ionomers affected the structure of clusters in the catalyst ink. Low-temperature SEM observation showed that with the increase of the mass fraction of 1-propanol (NPA) in the solvent, Pt/C clusters tended to coarsen, and the ionomer dispersed in the catalyst ink to form a network structure different from the ionomer in the solvent. Yamaguchi et al.[26] studied the effect of water/alcohol composition on the behavior of ionomers by using dynamic light scattering (DLS), small-angle X-ray scattering (SAXS), and ^{19}F nuclear magnetic resonance (NMR) spectroscopy. It is proved that 1-propanol/water can more effectively inhibit the change of the characteristic length of the rod ionomer and the selective solvation behavior of the rod ionomer than ethanol/water and clarify the influence of the Nafion dispersion state on the performance of the proton exchange membrane fuel cell. The above-mentioned studies show that the dispersion state of ionomers strongly depends on the physical properties of solvents. Sharma et al.[21] studied the particle size distribution of catalyst ink clusters in different alcohol solvents, indicating that the hydrodynamic diameter of clusters is the smallest in ethanol solvents. Yang et al.[27] used ultrasmall-angle X-ray scattering and cryo-TEM technology to study that the agglomeration behavior of the carbon carrier in the ink is affected by the interaction of solvent and the ionomer on the carbon carrier. Khandavalli et al.[28] studied the rheological properties and cluster morphology of carbon suspension and the catalyst ink with different IC ratios by rheology and USAXS−SAXS technology. The results show that the interaction of the ionomer with the carbon carrier and the Pt crystal has an important effect on the rheological properties and the cluster structure of inks. Park et al.[16] studied the morphology of different carbon-supported catalysts in the ink by the STEM and N_2 adsorption technology. It was found that the specific surface area and the pore structure of the carbon support affected the adsorption of the ionomer on the catalyst surface, and the morphology of the cluster structure depended on the structure of the carbon support. In conclusion, the interaction between the solvent, ionomer, and catalyst in inks is a non-negligible factor to determine the structure and characteristics of clusters in the ink.

In this paper, the properties of ionomers and the dispersion of clusters in the ink in different solvents were studied. The relative viscosity, ζ-potential, effective proton fraction, relative mobility of the main chain, and the side chain of the ionomer were studied by rheometer, particle potentiometric titrator, acid−base titration, and nuclear magnetic resonance. The extension state of the ionomer in solvent was analyzed. The rheological properties of the fresh ink (10 wt %) were studied with a rotating rheometer. The network structure of clusters in the ink and the fragmentation and reconstruction behavior of clusters in the ink were studied by the viscosity curve, amplitude scanning, and 3ITT test. The solid content of the ink is diluted to 1 wt %. The particle size distribution of clusters in the ink was characterized by DLS technology. The interaction between clusters in a dilute solution was analyzed by the viscosity curve and amplitude scanning. Finally, the effects of solvent characteristics and ionomer dispersion on clusters in the ink were clarified (Table 1).

Table 1. Solubility and the Dielectric Constant of Pure Solvent and Ionomer[29,30a]

	Water	IPA	NPA	ET	Main chain	Side chain
Solubility parameters δ	23.4	11.5	11.9	12.9	9.1	17.3
Dielectric constant ε	78.4	18.3	22.2	23.8		

[a]Influence of the composition of isopropyl alcohol/water mixture solvents in catalyst ink solutions on the proton exchange membrane fuel cell performance. Copyright [2013] [Journal of Power Sources/Trung Truc Ngo] [New Preparation Method for Polymer-Electrolyte Fuel Cells]. Copyright [1995] [The Electrochemical Society/Makoto Uchida].

2. RESULTS AND DISCUSSION

The dispersion state of ionomers with different solvents was determined by the relative viscosity test, ζ-potential test, and effective proton number test. According to the principle of similar phase solubility, the closer the solubility of the main chain and the side chain of the ionomer to that of the solvent, the more it can promote the dissolution of the main chain of the ionomer in a solvent.[29,31] At the same time, the ionization degree of $-SO_3H$ on the side chain of the ionomer will increase with the increase of the solvent dielectric constant. Figure 1 shows that the relative viscosities of ionomers dispersed in water, 50 wt % IPA, 50 wt % NPA, and 50 wt % ET are 3.12, 3.84, 3.91, and 3.72, respectively. On the whole, the relative viscosity of ionomers in an alcohol aqueous solution is greater than that in a pure aqueous solvent. The main chain and the side chain of the ionomer will dissolve in the solvent, and the anion group generated by $-SO_3H$ on the side chain after electrolysis will provide Coulomb force.[32] According to x-DLVO theory, when clusters are close to each other, the Coulomb force and steric hindrance on the cluster surface will inhibit the aggregation of clusters. ζ-Potential of ionomer dispersion shows that the ζ-potential of the ionomer in water is −61.6 mV. In addition, in the aqueous solvent of alcohol, the ζ-potential of ionomer clusters increases with the increase of the dielectric constant of alcohol. The test results of the effective proton fraction of ionomer dispersion show that the effective proton fractions of the ionomer in water,[23] 50 wt % IPA, 50 wt % NPA, and 50 wt % ET are 62.87, 46.72, 49.35, and 53.66%, respectively. Therefore, the larger the dielectric constant of the solvent, the more ionization of $-SO_3H$ on the side chain extending into the solvent. Because the solubility parameters of water are quite different from those of the main chain of the ionomer, it is not conducive to the

https://doi.org/10.1021/acsomega.1c05026
ACS Omega 2021, 6, 32960−32969

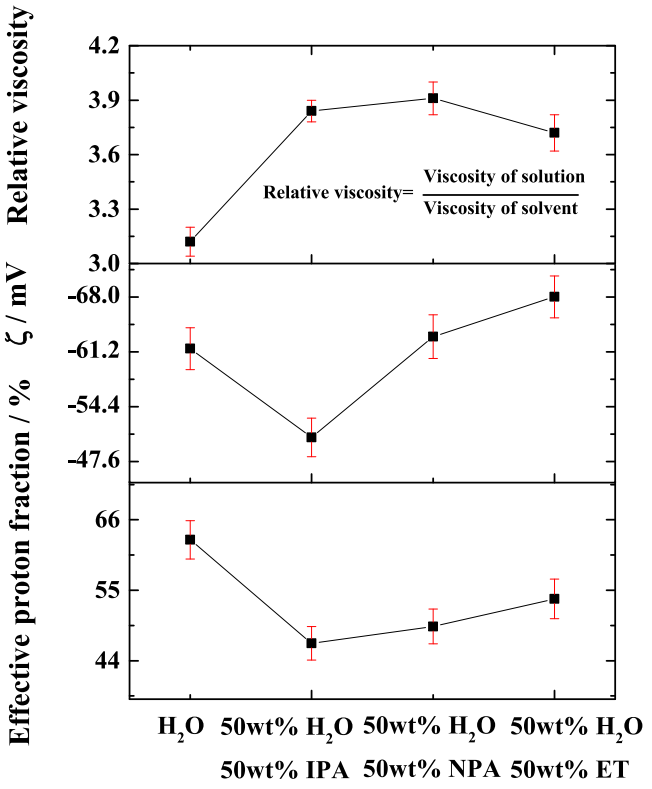

Figure 1. Relative viscosity, ζ-potential, and effective proton fraction of the ionomer in different solvents.

depolymerization of the main chain of the ionomer. The main chain agglomeration of the ionomer is due to the hydrophobic interaction, while $-SO_3H$ has better hydrophilicity, which makes it easier to dissociate to water.[23,33] The ionomer has a smaller effective proton fraction in the alcohol−water solution, indicating that the degree of $-SO_3H$ dissociation is high. Although alcohols can promote the dissolution of the main chain of the ionomer and lead to the extension of the side chain into the solvent, alcohols have a lower dielectric constant, which is not conducive to electrolytic dissociation of $-SO_3H$ on the side chain of the ionomer. In addition, $-SO_3H$ is more hydrophilic than alcohols, so the effective proton fraction in an alcohol−water solvent is relatively small.

To clarify the effect of solvent on the dispersion state of ionomers, NMR was used to quantitatively calculate the mobility of the main chain and the side chain of ionomers in different solvents. The main chain of the ionomer is poly(tetrafluoroethylene) (solubility parameters δ = 9.1), and the side chain is polar molecules with −O− and $-SO_3H$ (solubility parameters δ = 17.3).[34] In the original ionomer solution (D2020, 20 wt % Nafion), large clusters are formed due to secondary agglomeration. The solvent with close solubility to the main chain of the ionomer is conducive to the agglomeration of clusters, and the interaction between water molecules with higher solubility and side chains is stronger, which is conducive to the extension of side chains of ionomers. The NMR test showed that, in a pure water solvent, the peaks 3, 5, and 6 (CF_3, OCF_2) of the ionomer coincided at −81 ppm. At −118 ppm, the intensity of peak 7 (SCF_2) is relatively smaller, indicating that the branching degree of the side chain is smaller (Figure 2b). It was verified by the acid−base titration experiment that the ionomer has a larger effective proton fraction in an aqueous solvent, which is due to the larger

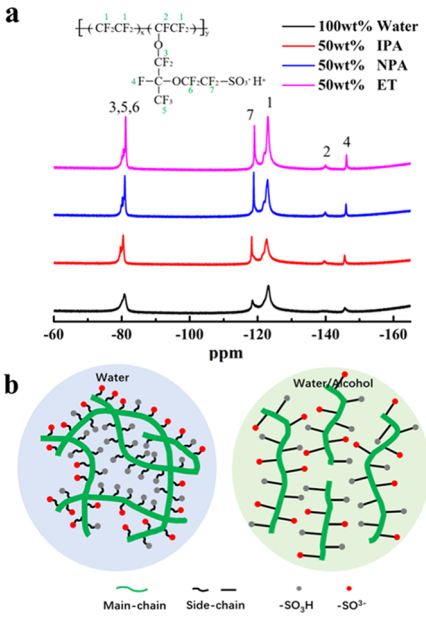

Figure 2. (a) NMR measurement of ionomers in different solvents and (b) dispersion state of the ionomer in a solvent.

dielectric constant of water (ε = 78.4). In alcohol/water solvent, the corresponding peak of the ionomer side chain is displayed, indicating that the side chain wrapped in the main chain stretches into the solvent. The ionomer dispersion with higher branching degree has a stronger interaction with the solvent. Due to the Coulomb force, more water molecules and alcohol molecules in the solvent will interact with the side chain of the ionomer to form new polymers. The ionomer with a complex structure will lead to the increase of the dispersion relative viscosity of the ionomer. In contrast, the relative viscosity of the ionomer in ethanol aqueous solution is smaller, which may be due to the fact that isopropanol and n-propanol have a more complex molecular structure, and the formed polymer has a more complex structure, which increases the relative viscosity of ionomer dispersion.

The rheological properties of the ink with a solid content of 10 wt % were tested, and the viscosity and flow curves of the ink were obtained (Figure 3). The test results show that ink-1 has the maximum viscosity at a low shear rate (0.1 s^{-1}), indicating that the ink has the maximum flow friction,[35] which may come from large clusters and the strong network strength. At a high shear rate (1000 s^{-1}), the viscosities of ink-1, ink-2, and ink-3 are similar and decrease in turn, indicating that the larger clusters in the ink form smaller clusters under the hydrodynamic action. Ink-1 shows the maximum viscosity in the whole shear process. Shear thinning occurs within the shear rate range of 0.1−10 s^{-1}, large clusters are broken,[36,37] and then a viscosity platform area appears within 10−30 s^{-1}, which is jointly determined by the fragmentation of clusters in the ink, the ordering of particle arrangement, and Brownian motion.[38−42] The flow curve of ink1 shows that the region with a shear rate between 0.1 and 10 s^{-1} is a pseudoplastic region. At this time, the orientation of clusters in the ink is ordered, the destruction and decomposition ability of clusters is greater than that of mutual crosslinking, and the viscosity decreases. The shear rate is the platform area within 10−30 s^{-1}, the slope of the curve is equal to 1, and the ink behaves as Newtonian flow. Then, with the increase of the shear rate, the ink

https://doi.org/10.1021/acsomega.1c05026
ACS Omega 2021, 6, 32960−32969

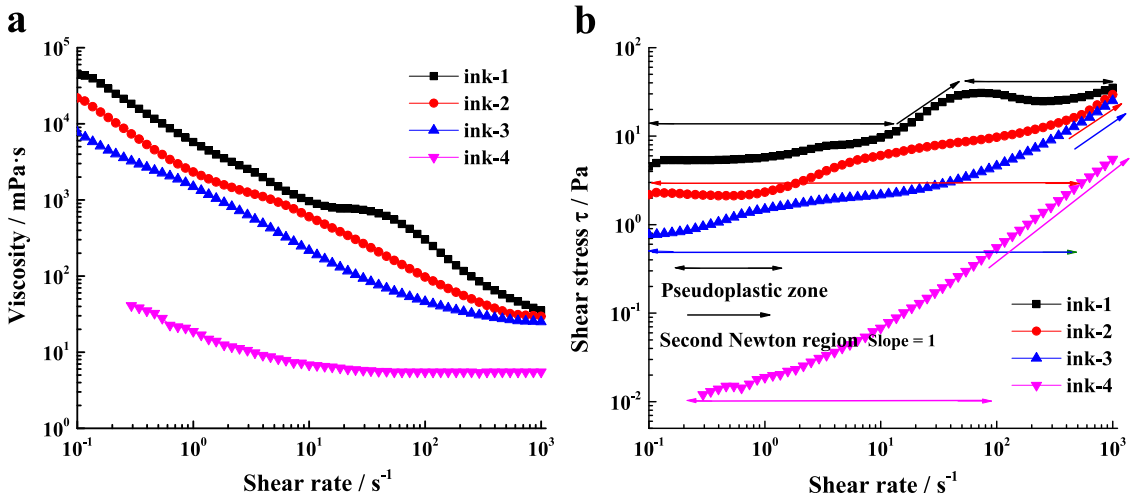

Figure 3. (a) Viscosity curve and (b) the flow curve of the ink prepared with different solvents.

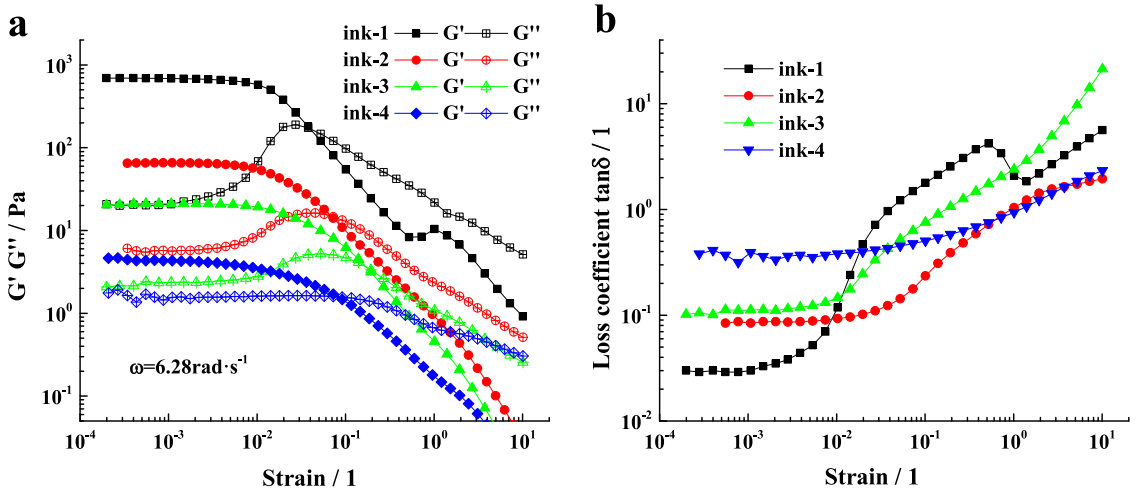

Figure 4. (a) Amplitude scanning curve and (b) the loss coefficient curve of the ink with different solvents.

continues to show shear thinning behavior. The shear-thinning behavior of ink-2 and ink-3 occurred continuously during the shear process, and the phenomenon in the platform region was weak. It entered the second Newton region only after the shear rate was greater than 400 s^{-1}. The shear thinning of ink-4 occurs within 0.1−100 s^{-1}. With the increase of the shear rate, the viscosity continues to decrease, showing pseudoplastic fluid behavior. When the shear rate is greater than 100 s^{-1}, it indicates that the crosslinking between clusters in the ink has no time to rebuild and the viscosity value has been the smallest, showing the Newtonian flow.

Amplitude scanning is used to test the strength of the network structure in inks (Figure 4). Corresponding to the viscosity curve, the higher the viscosity, the greater the storage modulus, indicating that the ink has a stronger network structure.[43,44] The linear plateau region (LVE) occurs when the shear strain is between 10^{-4} and 10^{-2}. Under the action of shear stress, the network structure in the LVE ink changed elastically, and the structure was basically not damaged. The storage modulus curve and the loss modulus curve of ink-1 change very rapidly after the shear stress exceed the LVE region, indicating that the damage of the network structure in ink-1 is completed quickly. After the network structure in ink-1 is destroyed, more new structures will not be formed immediately. The solid characteristics in the ink disappear rapidly and begin to show a liquid viscosity behavior. When the shear strain of other inks exceeds the LVE region, the storage modulus changes slowly. While the internal network of ink is destroyed, more new structures will be produced, which makes the change from solid characteristics to liquid characteristics more slow. With the increase of shear strain, the storage modulus curve intersects with the loss modulus curve, the fluid begins to flow and the loss coefficient corresponding to the flow point is 1.

The fragmentation and recombination of clusters, the destruction, and generation of the network structure in the ink were tested by 3ITT (Figure 5). When the shear rate is 0.1 s^{-1}, the viscosity of the ink is relatively stable, the clusters in the ink are not broken and the network structure is not damaged. When the shear rate increases to 100 s^{-1}, it shows that the clusters in the ink have begun to break, and the network structure in the ink has been damaged. At the same time, the hydrodynamic action makes the cluster arrangement orderly, which reduces the flow friction in the ink and leads to the decrease of ink viscosity. In the third test, when the shear rate is 0.1 s^{-1}, the role of the shear force in the ink can be ignored, and the broken clusters can no longer maintain an orderly arrangement under the action of the Brownian motion.

https://doi.org/10.1021/acsomega.1c05026
ACS Omega 2021, 6, 32960−32969

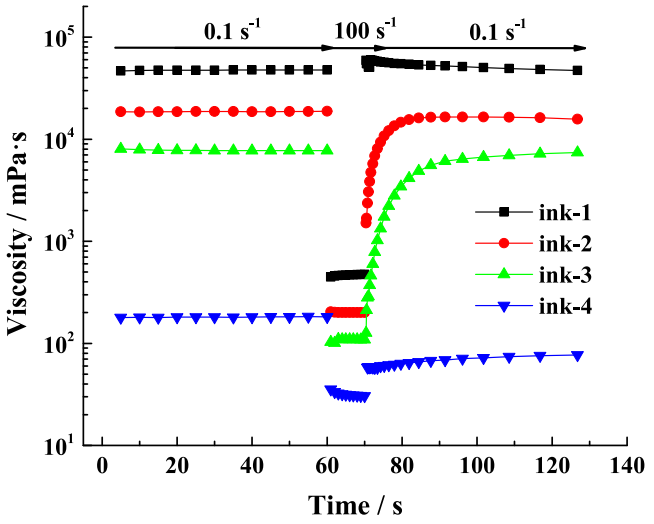

Figure 5. 3ITT test of inks with different solvents.

Under the action of van der Waals force, the broken particles gradually agglomerate to form large clusters, and the new network structure gradually begins to be generated, increasing the flow friction in the ink. Therefore, during the third test, the viscosity of ink-2 and ink-3 increased slowly between 70 and 80 s. However, after the shear force is removed, the viscosity of ink-1 immediately returns to the initial state, indicating that the interaction between clusters in ink-1 is stronger, and the cluster particles can reunite immediately to form new aggregates and network structures. In ink-4, when the shear force is removed, the broken particles will not agglomerate quickly and form a new network structure, resulting in the inability of the ink viscosity to return to the initial state.

Figure 6 is a TEM diagram of a cluster structure in the ink. Figure 6a shows that the cluster agglomeration in the ink is more serious and the density of the cluster structure is greater, which shows that the cluster particles are more difficult to break and the connection between clusters is stronger in water. Figure 6b,c shows the morphology and structure of clusters in a water/alcohol solvent. The agglomeration behavior between clusters is weakened, resulting in the decrease of cluster structure density and the increase of pores. In addition, branching occurs at the edge of the cluster, indicating that the cluster is dispersed and the particle size decreases in water/alcohol solvent. In contrast, the catalyst clusters in water/ethanol solvent are more dispersed and have larger pores,

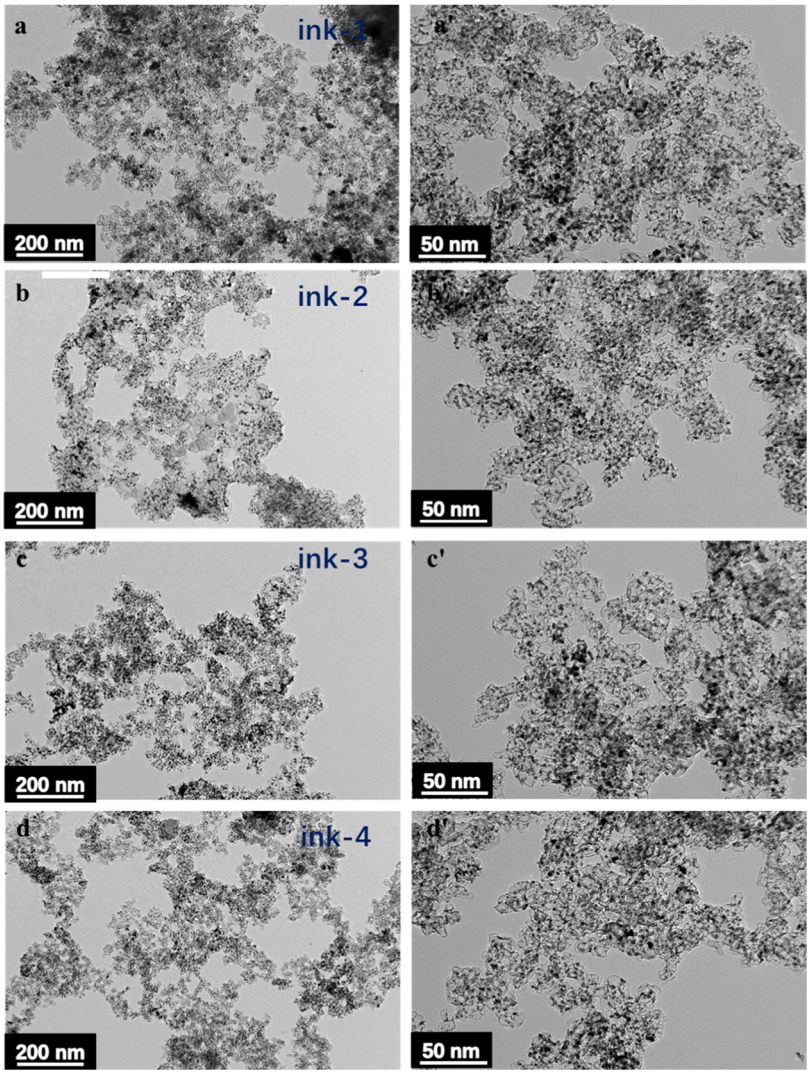

Figure 6. TEM test of clusters in the ink with different solvents: (a, a′) water; (b, b′) 50 wt % IPA; (c, c′) 50 wt % NPA; (d, d′) 50 wt % ET.

https://doi.org/10.1021/acsomega.1c05026
ACS Omega 2021, 6, 32960−32969

indicating that the clusters are more fully dispersed and the particle size is smaller. Corresponding to the rheological curve, in ink-1, the particle size of clusters is larger and the connection between clusters is stronger, resulting in greater viscosity and stronger storage modulus. In ink-2 and ink-3, the particle size of clusters decreases, the branching behavior of clusters decreases, the connection strength decreases, and the viscosity and storage modulus decrease. In ink-4, the particle size of clusters is the smallest, the porosity between clusters is the largest, and the connection between clusters is the weakest, resulting in minimum viscosity and storage modulus.

The Coulomb force and van der Waals force on the particle surface jointly determine the agglomeration behavior of particles in the ink. When clusters collide under Brownian motion and van der Waals force, if the total potential energy of clusters is greater than the activation energy of particle adsorption, secondary agglomeration occurs. According to the hypothesis of x-DLVO theory, the activation energy of cluster adsorption is determined by the electrostatic repulsion and the steric hindrance provided by the ionomer on the cluster surface.[24] The ζ-potential test of the ink shows that the ζ-potentials of the cluster surface in ink-1, ink-2, ink-3, and ink-4 are −188.5, −156.3, −132.7, and −73.6 mV, respectively, indicating that the electrostatic repulsion in ink-1 is stronger, which will lead to the increase of adsorption activation energy (Figure 7). However, the viscosity test shows that there are

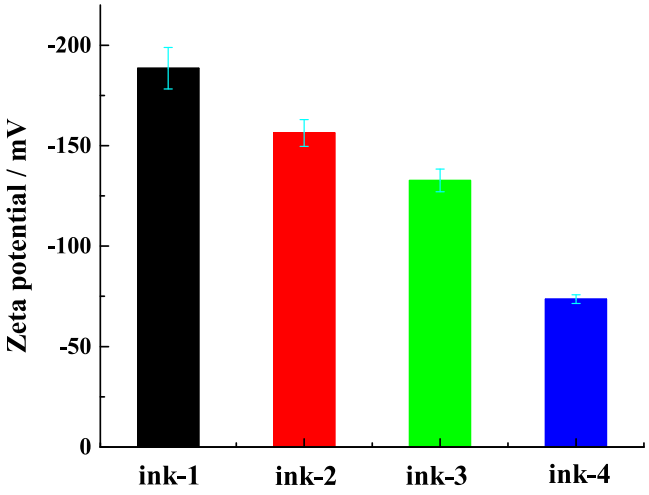

Figure 7. ζ-Potential of the cluster surface in the ink with different solvents.

maximum and minimum cluster diameters in ink-1 and ink-4, respectively, indicating that the ionomer in ink-4 provides greater steric hindrance than that in ink-1. The NMR test shows that the diameter of ionomer clusters in pure water is larger, which cannot be immersed into the cluster pores to disperse the clusters and cannot provide more steric hindrance. In ink-2, ink-3, and ink-4, the ζ-potential on the cluster surface is lower, but smaller ionomer particles can fully invade the cluster, making the ionomer more evenly adsorbed on the cluster surface and reducing the cluster particle size.[45] In addition to the role of the ionomer, the type of solvent also plays an important role in the dispersion of clusters. Alcohol solvent has lower surface tension and is more likely to invade into the pores of catalyst aggregates to disperse the clusters.

To eliminate the influence of steric hindrance on the agglomeration behavior of clusters in ink to a greater extent, the rheological properties of ink diluted to 1 wt % were tested.[46] The viscosity curves showed that the viscosities of ink-1D, ink-2D, ink-3D, and ink-4D decreased in turn. At a low shear rate ($0.1\ s^{-1}$), ink-1D has the highest viscosity, indicating that there is still a strong spatial network structure and larger clusters in the ink. At a high shear rate ($1000\ s^{-1}$), the viscosity of ink-1 is greater, indicating that the particle size of clusters in ink is larger. The physical characterization of ionomer dispersion shows that the dispersion state of the ionomer in 50 wt % IPA and 50 wt % NPA is similar, so the rheological properties of ink-2D and ink-3D show similar phenomena. In 50 wt % ET, the ionomer has a smaller cluster particle size and a smaller molecular structure of ethanol, which is easy to invade into the catalyst cluster and make the catalyst cluster more dispersed. Figure 8b flow curve shows that the shear stress of ink-1D hardly changes with the increase of the shear rate during the whole test process, indicating that the clusters in the ink continue to break under the action of hydrodynamic force, showing shear thinning behavior.[37,47] In the flow curve of ink-4D, the shear stress is positively correlated with the shear rate, showing the behavior of a Newtonian fluid.[48]

To study the strength of the network structure in the diluted ink, the ink was tested by amplitude scanning. After ink dilution, the solid content and steric hindrance of the ink will be reduced, and the influence of the network structure on the study of cluster behavior will be reduced.[43] The amplitude scanning test shows that the storage modulus in all inks decreases, the storage modulus of ink-1D in the LVE region is close to the loss modulus, and the fluid behavior is at the critical point of solid behavior and liquid behavior. The loss modulus of ink-2D, ink-3D, and ink-4D in the LVE region is greater than the storage modulus, showing the viscous behavior of liquid, which basically eliminates the influence of the network structure on the ink. Figure 8b shows the test of loss coefficient in the ink. The loss coefficient of the diluted ink increases, the loss coefficient of ink-1D is close to 1, while the loss coefficients of ink-2D, ink-3D, and ink-4D are greater than 1, showing liquid viscosity behavior.

ζ-Potential test and DLS test were carried out on the diluted ink. The test results show that the ζ-potential of ink-1D and ink-4D is higher because water and ethanol have greater dielectric constant and polarity, which can promote the electrolysis of $-SO_3H$ on the side chain of the ionomer and increase the charge density on the cluster surface. The DLS test shows that the hydrodynamic diameter D50 of clusters in ink-1D, ink-2D, ink-3D, and ink-4D decreases successively, the particle size distribution in ink-1D shows double peaks and larger clusters exist at 1000 nm (Figure 9). The particle size distributions of clusters in ink-2D and ink-3D are similar. In contrast, ink-2D has more particles between 100 and 200 nm. The clusters of ink-4D are concentrated at 300 nm and have the smallest D50. Compared with water molecules, alcohol molecules have smaller surface tension, which can better invade the pores of clusters and break large clusters. In the aqueous solutions of the three alcohols, the ζ-potential of ionomers in ethanol/water solvent is the highest, which can provide greater electrostatic repulsion and is more conducive to the separation between clusters. In addition, smaller ionomers can be drilled into the pores of the clusters and evenly adsorbed to the surface of the clusters, making the clusters more dispersed in the ink (Figure 10).

https://doi.org/10.1021/acsomega.1c05026
ACS Omega 2021, 6, 32960−32969

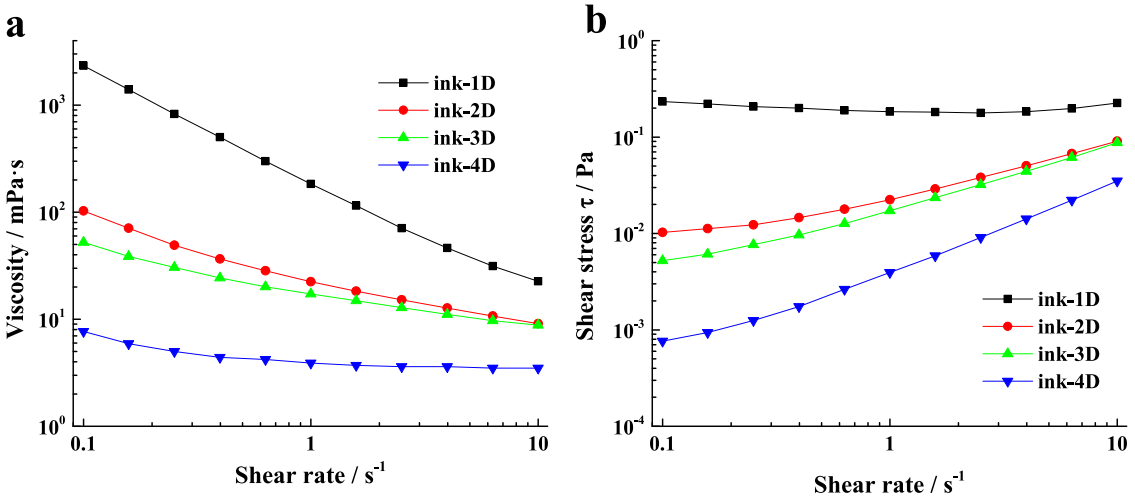

Figure 8. Ink with solid content of 1 wt %: (a) viscosity curve and (b) flow curve.

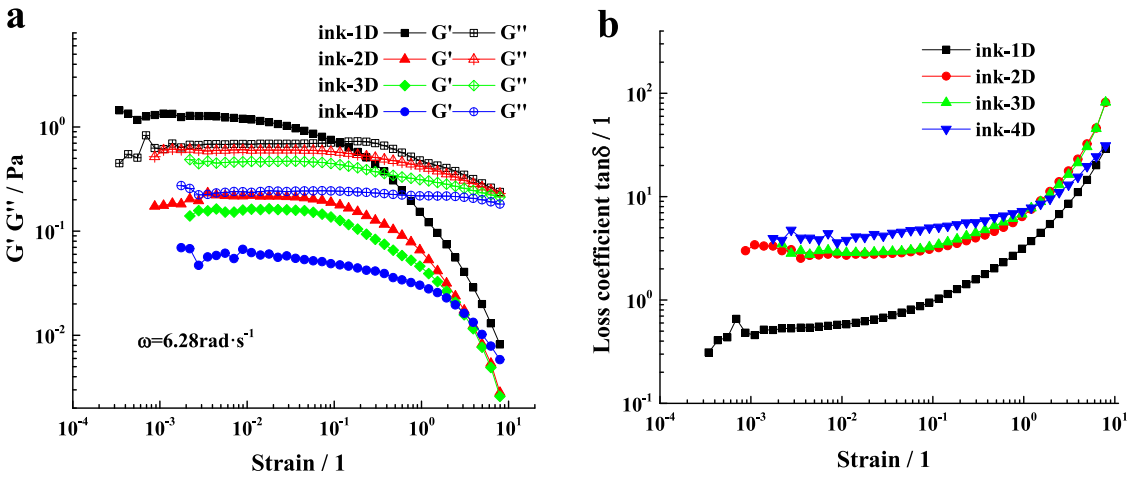

Figure 9. Ink with solid content of 1 wt %: (a) the amplitude scanning curve and (b) the loss coefficient curve.

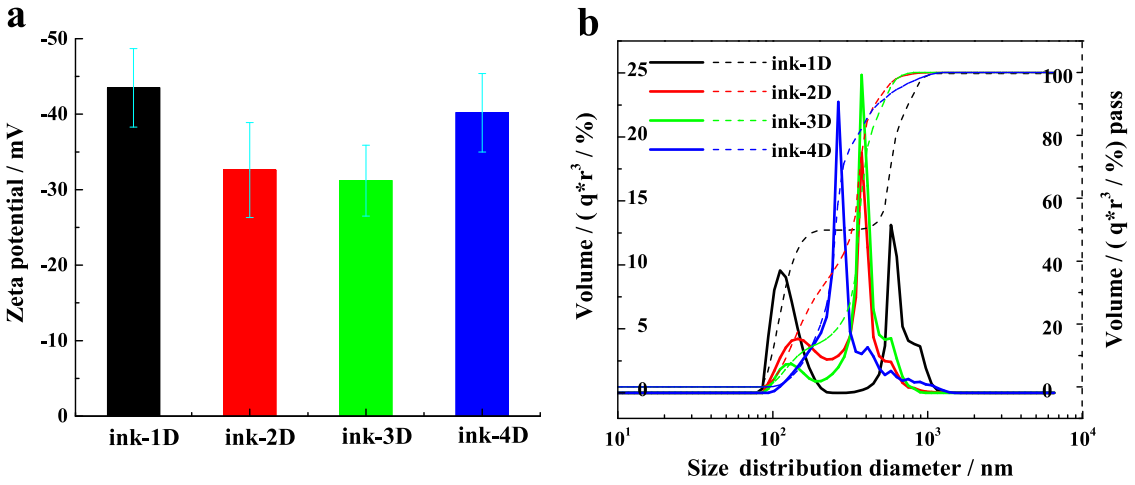

Figure 10. Ink with 1 wt % solid content: (a) ζ-potential on the cluster surface and (b) particle size distribution.

3. CONCLUSIONS

The factors affecting the cluster structure in the catalyst ink were studied. The results show that the structure of alcohol molecules in solvent and the dispersion state of the ionomer are the important factors affecting the structure of ink clusters and the strength of the network structure between clusters. The ionomer has higher dispersion and smaller cluster particle size in ethanol aqueous solvent. The rheological properties of 10 and 1 wt % inks were characterized. The results show that the network structure between clusters is stronger in 10 wt % inks. Moreover, the addition of alcohol could effectively reduce the particle size of clusters in the ink and the strength of the

https://doi.org/10.1021/acsomega.1c05026
ACS Omega 2021, 6, 32960−32969

network structure between clusters. The rheological test, DLS, and TEM test of 1 wt % solid content ink show that alcohol molecules with smaller molecular weight and ionomer clusters with smaller particle size are easier to enter the pores of catalyst clusters, promote the dispersion of clusters, reduce the particle size of ink clusters and the structural strength between clusters, and reduce the viscosity of the ink.

4. EXPERIMENT AND CHARACTERIZATION

The water−alcohol solvent is prepared as follows: deionized water and ethanol are used to prepare a water−ethanol mixture with a water content of 50 wt %. After ultrasonic treatment in a water bath for 5 s, the mixed water−alcohol solvent is obtained. The preparation of n-propanol aqueous solution and isopropanol aqueous solution is the same as the above scheme. The preparation of ionomer dispersion is as follows: use ionomer (D2020, 20 wt % Nafion), deionized water, and ethanol are used to prepare ionomer dispersion with an ionomer content of 2.5 wt % and water content of 50 wt % in a solvent. They are mixed evenly by ultrasonic treatment for 30 s. Different ionomer dispersions were prepared by replacing ethanol with *n*-propanol and isopropanol. The preparation of the catalyst ink is as follows: use 60 wt % Pt catalyst (Langsun), ionomer (20 wt % Nafion, D2020), deionized water, and ethanol are used to prepare the catalyst ink with a solid content of 10 wt %. The content of ionomer is 2.5 wt % (I/C = 0.833), and the contents of water and ethanol in solvent account for 50 wt %, respectively. First, deionized water was added to the catalyst and then the ionomer and ethanol were added. After ultrasonic mixing for 5 min, it was dispersed by high-speed shear for 60 min at 16 000 rpm. Different catalyst inks were prepared by replacing ethanol with *n*-propanol and isopropanol. The inks with solvents of 100 wt % water, 50 wt % IPA, 50 wt % NPA, and 50 wt % ET are recorded as ink-1, ink-2, ink-3, and ink-4, respectively; the ink solid content was diluted to 1 wt % with solvent and recorded it as ink1-D, ink2-D, ink3-D, and ink4-D, respectively.

For the rheological test, the viscosity of the suspension is tested and analyzed using a rotary rheometer (Anton Paar, MCR302) with a coaxial cylinder mold with double slits. During the test, the temperature is controlled to 25 ± 0.1 °C, the sample solution is presheared for 100 s under a shear rate of 40 s^{-1} to eliminate the residual stress, and the logarithmic points are taken in the shear rate range of 0.1−1000 s^{-1} for the viscosity curve test. The test range of the viscosity curve of catalyst inks with 1 wt % solid content is 0.1−10 s^{-1}. The viscosity of solvent and ionomer dispersion corresponds to the viscosity value at a shear rate of 10 s^{-1}, and the relative viscosity is equal to the viscosity of ionomer dispersion/the viscosity of the solvent. It is repeated three times and the average is taken. The strength of the network structure in the ink with a solid content of 10 and 1 wt % was tested by amplitude scanning. The temperature of the amplitude scanning test is 25 ± 0.1 °C, and the angular frequency is constant ω = 6.28 rad·s^{-1}, the shear strain ranges from 1 × 10^{-5} to 1; the elastic modulus and loss modulus of the network structure are tested in the ink. The fragmentation and reconstruction behavior of clusters and network structures in inks are analyzed by a three-stage thixotropy test (3ITT). The test temperature is 25 ± 0.1 °C, the preshear time is 100 s, and the shear rate is 40 s^{-1} to eliminate the residual stress of the sample. The fragmentation and reconstruction of clusters in the ink were tested in three stages. The clusters were sheared for 60 s at a shear rate of 0.1 s^{-1} to simulate the stationary state of the clusters; the fragmentation behavior of clusters and network structures was simulated by shearing for 10 s at a shear rate of 100 s^{-1}; the shear rate is 0.1 s^{-1}; it was sheared for 60 s. The viscosity of the ink was allowed to increase and then simulated the reconstruction behavior of clusters and network structure in the ink.

For the physical characterization of clusters, the ζ-potential of ionomer dispersion is tested by particle potentiometric titrator (Colloid Metrix, Stabino). The test temperature is 25 °C; 10 mL of the sample reagents is added to the cavity, tested five times, and the average value of ζ-potential is obtained. A cylindrical PTFE cavity and an oscillating piston are used. The surfaces of both have little negative ion charge. A small part of the particles in the cavity is fixed on the wall. With the movement of the piston, the ion cloud of the electric double layer of static particles is pushed up and down. The oscillating ion cloud will produce an alternating voltage, i.e., flow potential, between the two electrodes. The flow potential is directly proportional to the ζ-potential of the particles. The algorithm of DLS technology is calculated based on the Brownian motion of particles in solvent. Using the principle of backscattering light and out-of-phase Doppler frequency shift, combined with the mathematical processing model of dynamic tube light scattering, the error of test results is less than 1%. According to the EW value of D2020, the theoretical proton concentration C1 in ionomer dispersion is calculated. About 0.01 of mol/L NaOH solution is prepared and acid−base neutralization titration for ionomer was carried out. Bromocresol green is used as an acid−base indicator. When the dispersion color of the ionomer changes from yellow to blue, the titration is completed. The concentration C2 of ionized protons in ionomer dispersion was calculated, then the effective proton fraction = C2/C1, titration was repeated for three times, and the average value was calculated. The solid content of the ink was diluted to 0.01 wt %, and the cluster structure in the ink was observed by a transmission electron microscope (JEM-2100F). The diluted ink on the copper grid was dropped, and the freeze-drying equipment to quickly dry the ink to maintain the cluster state in the ink was used. After the copper grid with the ink was frozen in a liquid nitrogen container at −190 °C for 4 h, the ink frozen on the surface of the copper grid was vacuum dried at 130 °C for 5 h.

AUTHOR INFORMATION

Corresponding Authors

Pingwen Ming − *School of Automotive Studies, Tongji University (Jiading Campus), Shanghai 201804, China; Clean Energy Automotive Engineering Center, Tongji University (Jiading Campus), Shanghai 201804, China*; Email: pwming@tongji.edu.cn

Bing Li − *School of Automotive Studies, Tongji University (Jiading Campus), Shanghai 201804, China; Clean Energy Automotive Engineering Center, Tongji University (Jiading Campus), Shanghai 201804, China*; orcid.org/0000-0002-4449-2217; Email: libing210@tongji.edu.cn

Authors

Daozeng Yang − *School of Materials Science and Engineering, Dalian Jiaotong University, Dalian 116021, China*

Shaomin Zhu − *School of Materials Science and Engineering, Dalian Jiaotong University, Dalian 116021, China*

https://doi.org/10.1021/acsomega.1c05026
ACS Omega 2021, 6, 32960−32969

Yuqing Guo − *School of Automotive Studies, Tongji University (Jiading Campus), Shanghai 201804, China; Clean Energy Automotive Engineering Center, Tongji University (Jiading Campus), Shanghai 201804, China*
Haifeng Tang − *Great Wall Motor Co., Ltd., Baoding 071000 Hebei, China*
Daijun Yang − *School of Automotive Studies, Tongji University (Jiading Campus), Shanghai 201804, China; Clean Energy Automotive Engineering Center, Tongji University (Jiading Campus), Shanghai 201804, China*
Cunman Zhang − *School of Automotive Studies, Tongji University (Jiading Campus), Shanghai 201804, China; Clean Energy Automotive Engineering Center, Tongji University (Jiading Campus), Shanghai 201804, China;* orcid.org/0000-0002-5693-094X

Complete contact information is available at: https://pubs.acs.org/10.1021/acsomega.1c05026

Notes

The authors declare no competing financial interest.

■ ACKNOWLEDGMENTS

The authors appreciate the National Natural Science Foundation of China (No. 52176198) and the Program of Ministry of Science &Technology of China (No. 2020YFB0106601) for financial support.

■ REFERENCES

(1) Staffell, I.; Scamman, D.; Velazquez Abad, A.; Balcombe, P.; Dodds, P. E.; Ekins, P.; Shah, N.; Ward, K. R. The role of hydrogen and fuel cells in the global energy system. *Energy Environ. Sci.* **2019**, *12*, 463−491.
(2) Wang, Y.; Ruiz Diaz, D. F.; Chen, K. S.; Wang, Z.; Adroher, X. C. Materials, technological status, and fundamentals of PEM fuel cells − A review. *Mater. Today* **2020**, *32*, 178−203.
(3) Hickner, M. A.; Ghassemi, H.; Kim, Y. S.; Einsla, B. R.; McGrath, J. E. Alternative Polymer Systems for Proton Exchange Membranes (PEMs). *Chem. Rev.* **2004**, *104*, 4587−4612.
(4) Litster, S.; McLean, G. PEM fuel cell electrodes. *J. Power Sources* **2004**, *130*, 61−76.
(5) Holdcroft, S. Fuel Cell Catalyst Layers: A Polymer Science Perspective. *Chem. Mater.* **2014**, *26*, 381−393.
(6) Viswanathan, V.; Hansen, H. A.; Rossmeisl, J.; Nørskov, J. K. Universality in Oxygen Reduction Electrocatalysis on Metal Surfaces. *ACS Catal.* **2012**, *2*, 1654−1660.
(7) Li, W.; Lin, R.; Yang, Y. Investigation on the reaction area of PEMFC at different position in multiple catalyst layer. *Electrochim. Acta* **2019**, *302*, 241−248.
(8) Russell, A. E. Electrocatalysis: theory and experiment at the interface. Preface. *Faraday Discuss.* **2009**, *140*, 9−10.
(9) Wang, X.; Zhou, B. Liquid water flooding process in proton exchange membrane fuel cell cathode with straight parallel channels and porous layer. *J. Power Sources* **2011**, *196*, 1776−1794.
(10) Salari, S.; Tam, M.; McCague, C.; Stumper, J.; Bahrami, M. The ex-situ and in-situ gas diffusivities of polymer electrolyte membrane fuel cell catalyst layer and contribution of primary pores, secondary pores, ionomer and water to the total oxygen diffusion resistance. *J. Power Sources* **2020**, *449*, No. 227479.
(11) Zhang, S.; Zhang, J.; Zhu, Z.; Liu, P.; Cao, F.; Chen, J.; He, Q.; Dou, M.; Nan, S.; Lu, S. Unusual influence of binder composition and phosphoric acid leaching on oxygen mass transport in catalyst layers of high-temperature proton exchange membrane fuel cells. *J. Power Sources* **2020**, *473*, No. 228616.
(12) Cheng, X.; Wei, G.; Wang, C.; Shen, S.; Zhang, J. Experimental probing of effects of carbon support on bulk and local oxygen transport resistance in ultra-low Pt PEMFCs. *Int. J. Heat Mass Transfer* **2021**, *164*, No. 120549.
(13) Woo, S.; Lee, S.; Taning, A. Z.; Yang, T.-H.; Park, S.-H.; Yim, S.-D. Current understanding of catalyst/ionomer interfacial structure and phenomena affecting the oxygen reduction reaction in cathode catalyst layers of proton exchange membrane fuel cells. *Curr. Opin. Electrochem.* **2020**, *21*, 289−296.
(14) Huang, D.-C.; et al. Effect of Dispersion Solvent in Catalyst Ink on Proton Exchange Membrane Fuel Cell Performance. *Int. J. Electrochem. Sci.* **2011**, *6*, 2551−2565.
(15) Andersen, S. M.; Borghei, M.; Dhiman, R.; Ruiz, V.; Kauppinen, E.; Skou, E. Adsorption Behavior of Perfluorinated Sulfonic Acid Ionomer on Highly Graphitized Carbon Nanofibers and Their Thermal Stabilities. *J. Phys. Chem. C* **2014**, *118*, 10814−10823.
(16) Park, Y.-C.; Tokiwa, H.; Kakinuma, K.; Watanabe, M.; Uchida, M. Effects of carbon supports on Pt distribution, ionomer coverage and cathode performance for polymer electrolyte fuel cells. *J. Power Sources* **2016**, *315*, 179−191.
(17) So, M.; Ohnishi, T.; Park, K.; Ono, M.; Tsuge, Y.; Inoue, G. The effect of solvent and ionomer on agglomeration in fuel cell catalyst inks: Simulation by the Discrete Element Method. *Int. J. Hydrogen Energy* **2019**, *44*, 28984−28995.
(18) Tangsathitkulchai, C. Acceleration of particle breakage rates in wet batch ball milling. *Powder Technol.* **2002**, *124*, 67−75.
(19) Saheki, A.; Seki, J.; Nakanishi, T.; Tamai, I. Effect of back pressure on emulsification of lipid nanodispersions in a high-pressure homogenizer. *Int. J. Pharm.* **2012**, *422*, 489−494.
(20) Pollet, B. G.; Kocha, S. S. Using Ultrasound to Effectively Homogenise Catalyst Inks: Is This Approach Still Acceptable? *Johnson Matthey Technol. Rev.* **2022**, *66* (1). DOI: 10.1595/205651321X16196162869695
(21) Sharma, R.; et al. Influence of dispersion media on Nafion ionomer distribution in proton exchange membrane fuel cell catalyst carbon support. *Mater. Chem. Phys.* **2019**, *226*, 66−72.
(22) Welch, C.; Labouriau, A.; Hjelm, R.; Orler, B.; Johnston, C.; Kim, Y. S. Nafion in Dilute Solvent Systems: Dispersion or Solution? *ACS Macro Lett.* **2012**, *1*, 1403−1407.
(23) Berlinger, S. A.; McCloskey, B. D.; Weber, A. Z. Inherent Acidity of Perfluorosulfonic Acid Ionomer Dispersions and Implications for Ink Aggregation. *J. Phys. Chem. B* **2018**, *122*, 7790−7796.
(24) Lazzari, S.; Nicoud, L.; Jaquet, B.; Lattuada, M.; Morbidelli, M. Fractal-like structures in colloid science. *Adv. Colloid Interface Sci.* **2016**, *235*, 1−13.
(25) Shimanuki, J.; Takahashi, S.; Tohma, H.; Ohma, A.; Ishihara, A.; Ito, Y.; Nishino, Y.; Miyazawa, A. Microstructural observation of fuel cell catalyst inks by Cryo-SEM and Cryo-TEM. *J. Electron Microsc.* **2017**, *66*, 204−208.
(26) Yamaguchi, M.; Matsunaga, T.; Amemiya, K.; Ohira, A.; Hasegawa, N.; Shinohara, K.; Ando, M.; Yoshida, T. Dispersion of Rod-like Particles of Nafion in Salt-Free Water/1-Propanol and Water/Ethanol Solutions. *J. Phys. Chem. B* **2014**, *118*, 14922−14928.
(27) Yang, F.; Xin, L.; Uzunoglu, A.; Qiu, Y.; Stanciu, L.; Ilavsky, J.; Li, W.; Xie, J. Investigation of the Interaction between Nafion Ionomer and Surface Functionalized Carbon Black Using Both Ultrasmall Angle X-ray Scattering and Cryo-TEM. *ACS Appl. Mater. Interfaces* **2017**, *9*, 6530−6538.
(28) Khandavalli, S.; Park, J. H.; Kariuki, N. N.; Myers, D. J.; Stickel, J. J.; Hurst, K.; Neyerlin, K. C.; Ulsh, M.; Mauger, S. A. Rheological Investigation on the Microstructure of Fuel Cell Catalyst Inks. *ACS Appl. Mater. Interfaces* **2018**, *10*, 43610−43622.
(29) Ngo, T. T.; Yu, T. L.; Lin, H.-L. Influence of the composition of isopropyl alcohol/water mixture solvents in catalyst ink solutions on proton exchange membrane fuel cell performance. *J. Power Sources* **2013**, *225*, 293−303.
(30) Uchida, M.; Eda, N.; Ohta, A.; et al. New Preparation Method for Polymer-Electrolyte Fuel Cells. *J. Electrochem. Soc.* **1995**, *142*, 463−468.

(31) Ngo, T. T.; Yu, T. L.; Lin, H.-L. Nafion-based membrane electrode assemblies prepared from catalyst inks containing alcohol/water solvent mixtures. *J. Power Sources* **2013**, *238*, 1−10.
(32) Dobrynin, A.; Rubinstein, M. Theory of polyelectrolytes in solutions and at surfaces. *Prog. Polym. Sci.* **2005**, *30*, 1049−1118.
(33) Min, Z. et al. In *Brownian Dynamics Simulation of Branched Polymer Extensional Rheological Properties*, 2nd International Conference on Computer and Automation Engineering (ICCAE), 2010; pp 752−755.
(34) Kusoglu, A.; Weber, A. Z. New Insights into Perfluorinated Sulfonic-Acid Ionomers. *Chem. Rev.* **2017**, *117*, 987−1104.
(35) Woo, K.; Jang, D.; Kim, Y.; Moon, J. Relationship between printability and rheological behavior of ink-jet conductive inks. *Ceram. Int.* **2013**, *39*, 7015−7021.
(36) He, W.; Nan, J.; Li, H.; Li, S. Characteristic analysis on temporal evolution of floc size and structure in low-shear flow. *Water Res.* **2012**, *46*, 509−520.
(37) Brown, A. B. D.; Clarke, S. M.; Convert, P.; Rennie, A. R. Orientational order in concentrated dispersions of plate-like kaolinite particles under shear. *J. Rheol.* **2000**, *44*, 221−233.
(38) Bossis, G. The rheology of Brownian suspensions. *J. Chern. Phys.* **1989**, *91*, No. 1866.
(39) Wagner, N. J.; Brady, J. F. Shear thickening in colloidal dispersions. *Phys. Today* **2009**, *62*, 27−32.
(40) Mari, R.; Seto, R.; Morris, J. F.; Denn, M. M. Shear thickening, frictionless and frictional rheologies in non-Brownian suspensions. *J. Rheol.* **2014**, *58*, 1693−1724.
(41) Maranzano, B. J.; et al. The effects of particle size on reversible shear thickening of concentrated colloidal dispersions. *J. Chem. Phys.* **2001**, *114*, No. 10514.
(42) Bender, J.; Wagner, N. J. Reversible shear thickening in monodisperse and bidisperse colloidal dispersions. *J. Rheol.* **1996**, *40*, 899−916.
(43) Hobbie, E. K. Shear rheology of carbon nanotube suspensions. *Rheol. Acta* **2010**, *49*, 323−334.
(44) Aoki, Y.; Hatano, A.; Watanabe, H. Rheology of carbon black suspensions. I. Three types of viscoelastic behavior. *Rheol. Acta* **2003**, *42*, 209−216.
(45) Maranzano, B. J.; Wagner, N. J. The effects of interparticle interactions and particle size on reversible shear thickening: Hard-sphere colloidal dispersions. *J. Rheol.* **2001**, *45*, 1205−1222.
(46) Yoshimune, W.; Harada, M. Impact of Nonadsorbed Ionomer on Viscosity of Catalyst Inks for Polymer Electrolyte Fuel Cells. *Bull. Chem. Soc. Jpn.* **2020**, *93*, 302−307.
(47) Drabek, J.; Zatloukal, M.; Martyn, M. Effect of molecular weight on secondary Newtonian plateau at high shear rates for linear isotactic melt blown polypropylenes. *J. Non-Newtonian Fluid Mech.* **2018**, *251*, 107−118.
(48) Jogun, S. M.; Zukoski, C. F. Rheology and microstructure of dense suspensions of plate-shaped colloidal particles. *J. Rheol.* **1999**, *43*, 847−871.

https://doi.org/10.1021/acsomega.1c05026
ACS Omega 2021, 6, 32960−32969